



Exploring the “ L – σ ” Relation of H II Galaxies and Giant Extragalactic H II Regions Acting as Standard Candles

Yan Wu¹, Shuo Cao¹, Jia Zhang², Tonghua Liu¹, Yuting Liu¹, Shuaibo Geng¹, and Yujie Lian¹

¹ Department of Astronomy, Beijing Normal University, 100875, Beijing, People’s Republic of China; caoshuo@bnu.edu.cn, liutongh@mail.bnu.edu.cn

² School of Physics and Electrical Engineering, Weinan Normal University, Shanxi 714099, People’s Republic of China

Received 2019 September 1; revised 2019 November 15; accepted 2019 November 24; published 2020 January 15

Abstract

Cosmological applications of H II galaxies and giant extragalactic H II regions (GEHRs) to construct the Hubble diagram at high redshifts require knowledge of the “ L – σ ” relation of the standard candles used. In this paper, we study the properties of a large sample of 156 sources (25 high- z H II galaxies, 107 local H II galaxies, and 24 GEHRs) compiled by Terlevich et al. Using the cosmological distances reconstructed through two new cosmology-independent methods, we investigate the correlation between the H β emission-line luminosity L and the ionized gas velocity dispersion σ . The method is based on non-parametric reconstruction using the measurements of Hubble parameters from cosmic clocks, as well as the simulated data of gravitational waves from the third-generation gravitational wave detector (the Einstein Telescope, ET), which can be considered as standard sirens. Assuming the relation between emission-line luminosity and ionized gas velocity dispersion, $\log L(\text{H}\beta) = \alpha \log \sigma(\text{H}\beta) + \kappa$, we find that the full sample provides a tight constraint on the correlation parameters. However, similar analysis done on three different subsamples seems to support the scheme of treating H II galaxies and GEHRs with distinct strategies. Using the corrected “ L – σ ” relation for the H II observational sample beyond the current reach of Type Ia supernovae, we obtain values of the matter density parameter, $\Omega_m = 0.314 \pm 0.054$ (calibrated with standard clocks) and $\Omega_m = 0.311 \pm 0.049$ (calibrated with standard sirens), in the spatially flat Λ CDM cosmology.

Unified Astronomy Thesaurus concepts: Cosmological parameters (339); H II regions (694); Standard candles (1563)

1. Introduction

The Hubble diagram, which is directly related to luminosity distances, has provided a useful method to probe cosmological parameters (Riess et al. 1998; Perlmutter et al. 1999). In order to measure the luminosity distance, we always turn to luminous sources of known (or standardizable) intrinsic luminosity in the universe, such as Type Ia supernovae (Cao et al. 2011, 2015a; Cao & Liang 2013; Chen et al. 2015; Qi et al. 2018) and less accurate but more luminous gamma-ray bursts (Pan et al. 2015) in the role of “standard candles.” Powerful H II galaxies and extragalactic H II regions constitute a population that can be observed up to very high redshifts, reaching beyond feasible limits of supernova studies. Indeed, the power of modern cosmology lies in building up consistency rather than in single and precise experiments (Biesiada et al. 2010; Cao et al. 2015b; Ma et al. 2019), which indicates that every alternative method of restricting cosmological parameters is desired. It is known that H II galaxies and H II regions of galaxies could have very similar physical systems (Melnick et al. 1987; Wei et al. 2016), an outstanding feature of which are rapidly forming stars surrounded by ionized hydrogen. More specifically, H II galaxies and H II regions may exhibit indistinguishable optical spectra, i.e., strong Balmer emission lines in H α and H β due to the hydrogen ionized by the young massive star clusters (Searle & Sargent 1972; Bergeron 1977; Terlevich & Melnick 1981; Kunth & Östlin 2000).

A well-defined sample of H II galaxies with accurately measured flux density and the turbulent velocity of the gas could be useful for testing cosmological parameters such as the present-day matter density, cosmic equation of state, etc. (Siegel et al. 2005; Plionis et al. 2011). Concerning such

cosmological applications, the first method used for this purpose is of statistical nature. Essentially, the idea is to discuss the important phenomenon whereby as the mass of the starburst component increases, both the number of ionized photons and the turbulent velocity of the gas will increase. Therefore, one may naturally expect a quantitative relation between the luminosity $L(\text{H}\beta)$ in H β and the ionized gas velocity dispersion σ , which has triggered numerous efforts to use H II galaxies for this purpose (Terlevich & Melnick 1981; Chávez et al. 2014). The first attempt to determine a possible correlation between the luminosity $L(\text{H}\beta)$ and profile width for giant H II regions was presented in Melnick (1979), which was then extended to the luminosity–velocity dispersion relation satisfied by elliptical galaxies, bulges of spiral galaxies, and globular clusters (Terlevich & Melnick 1981). It was found in subsequent analysis (Melnick et al. 1987, 1988) that such an “ L – σ ” relation with small scatter can be used to determine cosmic distances independently of redshifts. More promising candidates in this context are H II galaxies (HII Gx) and giant extragalactic H II regions (GEHRs) that can be observed up to very high redshifts. Following the suggestion by Pettini et al. (1998), many authors have confirmed the validity of the “ L – σ ” correlation at higher redshifts (Melnick et al. 2000), which showed that HII Gx and GEHRs can be used as independent distance indicators at $z \sim 3$.

From the original “ L – σ ” calibration of a sample of five high- z H II galaxies covering the redshift range $2.1 < z < 3.4$ (Melnick et al. 1988), in combination with the measurements of flux density and turbulent gas velocity, Siegel et al. (2005) determined the best-fit value for the matter density parameter, $\Omega_m = 0.21^{+0.30}_{-0.12}$, in the framework of the flat Λ CDM model. A similar analysis was made by Plionis et al. (2011) concerning

the so-called Λ CDM cosmology (with constant dark-energy equation of state), using a revised zero-point of the original “ L – σ ” relation (Jarosik et al. 2011). While comparing the results from the previous “ L – σ ” relation, differences in central values of the best-fit cosmological parameters were also reported: $\Omega_m = 0.22^{+0.06}_{-0.04}$. The possible cosmological application of these HII Gx and GEHRs as standard candles has been extensively discussed in the literature (Fuentes-Masip et al. 2000; Bosch et al. 2002; Telles 2003; Siegel et al. 2005; Bordalo & Telles 2011; Plionis et al. 2011; Chávez et al. 2012, 2014; Mania & Ratra 2012; Wei et al. 2016). It was found that the H II galaxies provide a competitive source of luminosity distance to probe the acceleration of the universe. For instance, more recently, on a new sample of 156 sources compiled by Terlevich et al. (2015), Wei et al. (2016) have studied the possibility of utilizing HII Gx to carry out comparative studies between competing cosmologies, such as Λ CDM and the $Rh = ct$ universe (Melia 2007, 2013). However, it should be noted that cosmological application of the HII Gx and GEHR data requires good knowledge of the “ L – σ ” relation of the “standard candles” used. One of the major uncertainties was the typical value of the model parameters (α , κ) of the relation between emission-line luminosity and ionized gas velocity dispersion, $\log L(\text{H}\beta) = \alpha \log \sigma(\text{H}\beta) + \kappa$. In order to obtain cosmological constraints, some authors chose to take α and κ as statistical nuisance parameters (Wei et al. 2016). One should remember that the nuisance parameters characterizing the “ L – σ ” relation introduce considerable uncertainty to the final determination of other cosmological parameters. Having this in mind, properties of the HII Gx and GEHR data should be readdressed with the biggest sample to date (156 combined sources, including 25 high- z HII Gx, 107 local HII Gx, and 24 GEHRs) and taking into account reliable cosmological distance information based on current precise observations.

This encourages us to improve and develop the methodology further, based on the newly compiled sample of measurements of the Hubble parameter $H(z)$ (which represents a type of new cosmological standard clock) and the simulated data of gravitational waves from the third-generation gravitational wave detector (which can be considered as a standard siren). Compared with the previous works (Siegel et al. 2005; Plionis et al. 2011; Wei et al. 2016), the advantage of this work is that we achieve reasonable and compelling constraints on the “ L – σ ” relation in both the electromagnetic (EM) and gravitational wave (GW) windows, using luminosity distances covering the H II redshift range derived in two cosmological-model-independent methods. This paper is organized as follows. We briefly introduce our methodology and the corresponding observational data (H II, $H(z)$, and GW) in Section 2. Cosmological-model-independent constraints on the full sample and several subsamples are presented in Section 3. The cosmological application of the calibrated “ L – σ ” relation of H II regions is described in Section 4. Finally, the conclusions are presented in Section 5.

2. Observations

It is only quite recently that reasonable catalogs of H II galaxies and extragalactic H II regions containing more than 100 sources, with spectroscopic as well as astrometric data, have become available. In this work, we have considered the current observations for 156 H II objects compiled by Terlevich

et al. (2015). This data set is a larger sample of sources than used by Siegel et al. (2005) or Plionis et al. (2011) and with more complete high-redshift data than used by Melnick et al. (1988).

On the one hand, the first complete sample from low-redshift ($0.01 < z < 0.2$) H II galaxies selected from the Sloan Digital Sky Survey (SDSS) DR7 spectroscopic catalog is provided in Abazajian et al. (2009). It consists of 128 local H II galaxies satisfying the following well-defined selection criteria: (1) the lower limit of the equivalent widths of the strongest emission lines relative to the continuum is $\text{EW}(\text{H}\beta) > 50 \text{ \AA}$, in order to guarantee the dominating contribution of a single young starburst to the total luminosity, without contamination from the underlying older population and older clusters (Dottori 1981; Dottori & Bica 1981; Melnick et al. 2000; Chávez et al. 2014; Wei et al. 2016); (2) extra objects with highly asymmetric emission lines should not be included in the final sample (Chávez et al. 2014); (3) the upper limit of the velocity dispersion is imposed as $\log \sigma(\text{H}\beta) < 1.8 \text{ km s}^{-1}$, in order to exclude rotationally supported systems and/or objects with multiple young ionizing clusters from contributing to the total flux and affecting the line profiles (Chávez et al. 2014). When applying the former two criteria to the full sample, 14 objects are removed with the two cuts, while seven more are excluded due to their high velocity dispersion measurements. Therefore, we have the “benchmark” catalog comprising 107 local objects. On the other hand, we also use a combined sample of 25 high- z H II galaxies covering the redshift range $0.64 \leq z \leq 2.33$ (taken from the XShooter spectrograph at the Cassegrain focus of the ESO–VLT (Terlevich et al. 2015) and the literature (Erb et al. 2006a, 2006b; Masters et al. 2014)), as well as 24 giant H II regions in nine nearby galaxies (taken from Chávez et al. 2012), which satisfy the well-defined observational selection criteria listed above. See Melnick et al. (1987) for the measured velocity dispersions and global integrated $\text{H}\beta$ fluxes with corresponding extinction.

Full information about all 156 sources that remain after the aforementioned selection can be found in Table 1 of Wei et al. (2016), including source names, redshifts, categories, integrated $\text{H}\beta$ flux, and corrected velocity dispersion. We remark here that the final sample covers the redshift range $0 < z < 2.33$, which indicates its potential usefulness in cosmology at high redshifts. From an observational perspective, the reddening-corrected $\text{H}\beta$ flux is measured by fitting a single Gaussian to the long-slit spectra (Terlevich et al. 2015), with the reddening corrections derived from the published $E(B - V)$ using a standard reddening curve (Calzetti et al. 2000). The velocity dispersion inside the aperture can also be derived from the spectroscopic data. More specifically, one could obtain the velocity dispersion (σ_0) and the corresponding 1σ uncertainty from the FWHM measurement of the $\text{H}\beta$ and [O III] $\lambda 5007$ lines, i.e.,

$$\sigma_0 \equiv \frac{\text{FWHM}}{2\sqrt{2\ln(2)}}. \quad (1)$$

Following the strategy of Wei et al. (2016), the final corrected velocity dispersion is defined as

$$\sigma = \sqrt{\sigma_0^2 - \sigma_{\text{th}}^2 - \sigma_{\text{i}}^2 - \sigma_{\text{fs}}^2}, \quad (2)$$

with the thermal broadening (σ_{th}), instrumental broadening (σ_{i}), and fine-structure broadening (σ_{fs}). See Chávez et al. (2014) for

more detailed discussion of the thermal and instrumental broadening, while the fine-structure broadening is taken as $\sigma_{\text{fs}} = 2.4 \text{ km s}^{-1}$, following the suggestion provided in García-Díaz et al. (2008).

The test of the “ L - σ ” relation of the standard candles requires a statistically complete and well-characterized (homogeneous) sample. Our list includes a wide class of H II objects at different redshifts, so we will follow the previous procedure applied to compact radio sources (Cao et al. 2015c, 2017a, 2017b) and galactic-scale strong lensing systems (Cao et al. 2016) in that, besides the full combined sample, we will consider separately three subsamples: high- z HII Gx, local HII Gx, and GEHRs.

3. Methodology

Following the phenomenological model first proposed in Chávez et al. (2012) and later discussed in Chávez et al. (2014) and Terlevich et al. (2015), the emission-line luminosity of a source is related to its ionized gas velocity dispersion by

$$\log L(\text{H}\beta) = \alpha \log \sigma(\text{H}\beta) + \kappa, \quad (3)$$

where α is the constant slope parameter and κ represents the logarithmic luminosity at $\log \sigma(\text{H}\beta) = 0$. This is an empirical formula, whose scatter has been proved to be very small so that it can be effectively used as a luminosity indicator in cosmology (Chávez et al. 2012; Terlevich et al. 2015). Meanwhile, The $\text{H}\beta$ luminosity of the sources is estimated from their reddening-corrected flux density, which, assuming isotropic emission, reads

$$L(\text{H}\beta) = 4\pi D_L^2(z) F(\text{H}\beta), \quad (4)$$

where $F(\text{H}\beta)$ is the reddening-corrected $\text{H}\beta$ flux and $D_L(z)$ is the luminosity distance at redshift z .

The combination of Equations (3) and (4) implies that if we had reliable knowledge of cosmological distances at different redshifts, then we would get stringent constraints on the range of parameters α and κ describing H II sources. Compared with the previous procedure of simultaneously restricting (α , κ) with the cosmological parameter Ω_m (in the framework of Λ CDM, XCDM, and $Rh = ct$ cosmologies) (Wei et al. 2016), in this work we try to place stringent constraints on the “ L - σ ” relation in both the EM and GW windows, using luminosity distances covering the H II redshift range derived in two cosmological-model-independent methods. Note that the strong degeneracies between Ω_m and the two parameters characterizing the “ L - σ ” relation not only confirm that the cosmological parameters are not independent of the nuisance parameters, but also attest to the motivation of our calculation (Wei et al. 2016).

In order to set limits on α and κ , we turn to two catalogs of $D_L(z)$ separately by two different methods. In the EM window, we will use luminosity distances derived in a cosmological-model-independent way from $H(z)$ measurements using Gaussian processes (GPs) (Seikel et al. 2012a). As is well known, assuming the FLRW metric of a flat universe, the angular diameter distance can be written as

$$D_L(z) = (1+z) \int_0^z \frac{c \, dz}{H(z)}, \quad (5)$$

where c is the speed of light and $H(z)$ is the Hubble parameter at redshift z . The idea of cosmological application of the GP technique in general and with respect to $H(z)$ data can be traced

back to the paper of Holsclaw et al. (2010); since then it has been extensively applied in more recent papers to test the cosmological parameters (Cao et al. 2017a, 2018), spatial curvature of the universe (Cao et al. 2019; Qi et al. 2019a), and the speed of light at higher redshifts (Cao et al. 2017b). In this analysis, following the recent works of Zheng et al. (2019) inspired by GPs, we have reconstructed the $c/H(z)$ function from recent Hubble parameter measurements, including 41 data points from the method using galaxy differential ages and 10 data points from the method based on the radial size of baryon acoustic oscillations, and then derived $D_L(z)$ covering the redshift range of H II observations.³ See Qi et al. (2018) and Zheng et al. (2019) for details and reference to the source papers. The advantage of the GPs is that we do not need to assume any parameterized model for $H(z)$ while reconstructing this function from the data, which may provide more precise measurements of angular diameter distances at a certain redshift. We use the publicly available code called the GaPP (Gaussian Processes in Python)⁴ to reconstruct the profile of the $H(z)$ function up to the redshift $z=2.5$, and this can subsequently be used to reconstruct the luminosity distance.

The GP method uses some attributes of a Gaussian distribution, i.e., the reconstructed function $f(z)$ follows a Gaussian distribution with a mean value $\mu(z)$ and Gaussian error $\sigma(z)$ at each point z . In this process, the values of the reconstructed function evaluated at any two different points (z and \tilde{z}) are connected by a covariance function $k(z, \tilde{z})$, which depends only on a set of hyperparameters (ℓ and σ_f). Rather than the squared exponential covariance function widely used in the previous studies (Seikel et al. 2012a, 2012b; Yang et al. 2015; Cai et al. 2016; Qi et al. 2019a), we take the Matérn ($\nu = 9/2$) form for the covariance function:

$$k(z, \tilde{z}) = \sigma_f^2 \exp\left(-\frac{3|z - \tilde{z}|}{\ell}\right) \times \left[1 + \frac{3|z - \tilde{z}|}{\ell} + \frac{27(z - \tilde{z})^2}{7\ell^2} + \frac{18|z - \tilde{z}|^3}{7\ell^3} + \frac{27(z - \tilde{z})^4}{35\ell^4}\right], \quad (6)$$

where σ_f defines the overall amplitude of the correlation and ℓ gives a measure of its coherence length. The reliability of the reconstructed function can be guaranteed by the fact that the hyperparameters will be optimized by the GP with the observational data sets, which furthermore indicates that the reconstructed function is independent of the initial hyperparameter settings. In this analysis, an issue that needs clarification is the achievable estimation of the 1σ confidence region for the reconstructed function $c/H(z)$. Note that the 1σ confidence region depends on both the actual errors of individual data points ($\sigma_{c/H(z)}$) and the product $K_* K_*^{-1} K_*^T$. Here K_* is the covariance matrix at redshift z_* , which is calculated from the

³ The Hubble constant $H_0 = 67.3 \text{ km s}^{-1} \text{ Mpc}^{-1}$ from the latest Planck observations of the cosmic microwave background (CMB) (Planck Collaboration et al. 2018) is also taken for distance reconstruction in our analysis.

⁴ <http://www.acgc.uct.ac.za/~seikel/GAPP/index.html>

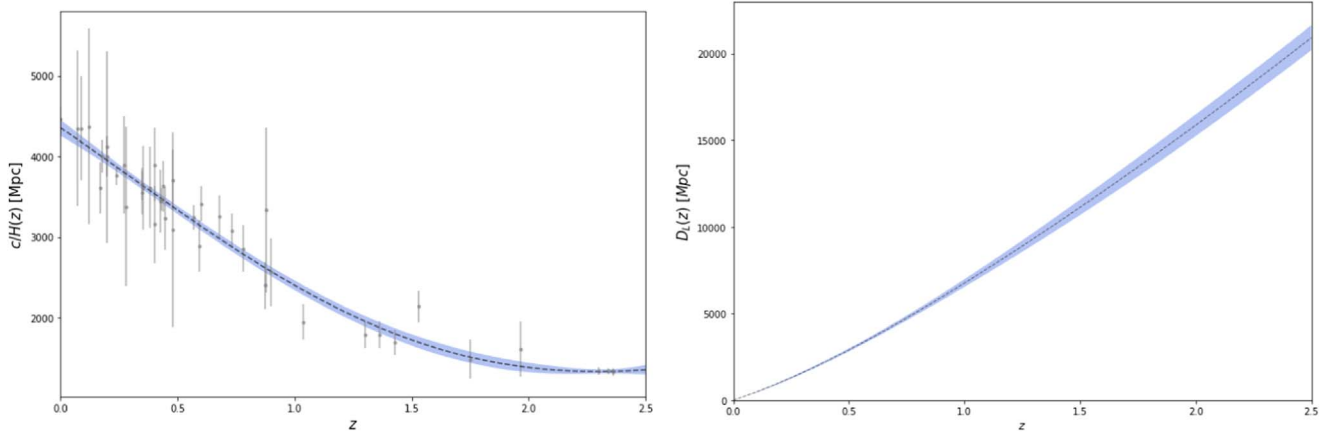


Figure 1. Left: recent measurements of the Hubble parameter (black points) and the reconstruction of the $c/H(z)$ function with the GP. Right: the corresponding reconstructed luminosity distance $D_L(z)$ with the GP (given the covariance matrix between the reconstructed $c/H(z)$ points). The blue region represents the 1σ confidence region.

original $c/H(z)$ data at z_i and the covariance matrix k :

$$K_* = [k(z_1, z_*), k(z_2, z_*), \dots, k(z_i, z_*)]. \quad (7)$$

It should be pointed out that, when there is a large correlation between the data ($K_* K_*^{-1} K_*^T > \sigma_f$), the dispersion at point z_i will be less than $\sigma_{c/H(z)}$ and the reconstructed 1σ regions will correspondingly become smaller. More specifically, it was shown in the previous analysis (Seikel et al. 2012a, 2012b) that the correlation between any two points z and \tilde{z} will be large only when $z - \tilde{z} < \sqrt{2}\ell$, which is clearly satisfied by the current $H(z)$ data used in our analysis. Therefore, as can be seen from the reconstructed results shown in Figure 1, the GP-estimated 1σ confidence region is much smaller than the uncertainties in the original $c/H(z)$ data. This issue has been extensively discussed in Seikel et al. (2012a). Using the reconstructed profile of the $c/H(z)$ function up to redshifts $z \sim 2.5$, we are able to reconstruct the luminosity distance $D_L(z)$ with the aforementioned GPs. One should note that the error band should be interpreted in a redshift-by-redshift sense and the covariances are not visible in such a plot (Seikel et al. 2012a). Following the commonly used procedure for transforming $c/H(z)$ data into luminosity distance (Holanda et al. 2013), the $D_L(z)$ function can be calculated by the usual simple trapezoidal rule (through Equation (5)). With the standard error propagation formula, the error associated with the i th redshift bin is given by $s_i = \frac{1}{2}(\sigma_{c/H(z_i)}^2 + \sigma_{c/H(z_{i+1})}^2)$, where $\sigma_{c/H(z)}$ is the error of the $c/H(z)$ data reconstructed from GPs. However, it should be noted that the constructed luminosity distances are correlated, since all of the derived s_i are statistically dependent on each other (Liao et al. 2015). More specifically, the $c/H(z)$ data are GP-reconstructed, following a multidimensional Gaussian distribution with the covariance matrix (through Equation (7)). Hence, the uncertainty of the luminosity distance corresponding to a certain redshift z should include statistical uncertainties and the covariances between every pair of $c/H(z)$ values among the total data. That is,

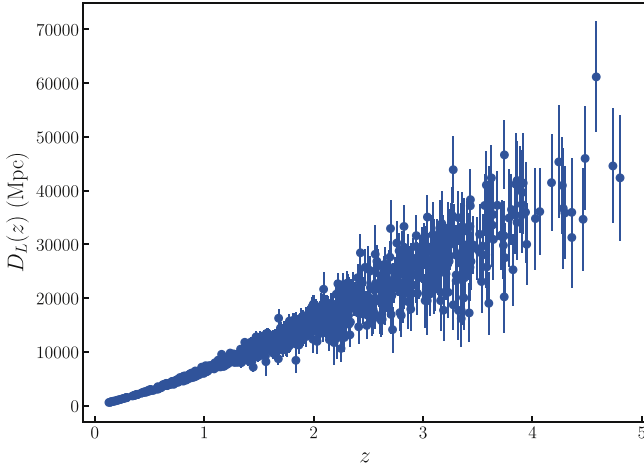
$$\sigma_{D_L(z)}^2 = \frac{(\Delta z)^2}{2} \left[\sum_{i=1}^n s_i + \sum_{i=2}^n \sum_{j=1}^{i-1} \text{Cov} \left(\frac{c}{H(z_i)}, \frac{c}{H(z_j)} \right) \right], \quad (8)$$

where Δz is the length of the redshift bin, while Cov denotes the covariance matrix for a set of reconstructed $c/H(z)$ points given by Equation (7). The results are also shown in Figure 1, where the reconstructed $D_{L,H(z)}$ function with corresponding 1σ uncertainty strip is displayed. Distance reconstruction with the Hubble parameter measurements is denoted as “Cosmology-independent method I.”

In the GW window, we turn to the simulated data of gravitational waves from the third-generation gravitational wave detector, which can be considered as a standard siren to provide information on the luminosity distance. GWs provide us with a completely new means of observation and are also a promising probe for cosmology. It is well known that the detection of GWs from the merger of a double compact object (DCO) (Abbott et al. 2016, 2017) has opened the new era of GW astronomy. The original idea of using the waveform signal to directly measure the luminosity distance D_L to the GW sources can be traced back to the paper of Schutz (1986), which indicates that inspiraling and merging compact binaries consisting of neutron stars (NSs) and black holes (BHs) can be used to constrain the Hubble constant by combining the redshift information on the source. Therefore, GW signals from the merger of DCOs are put forward as distance indicators and are called standard sirens (Dalal et al. 2006; Zhao et al. 2011; Taylor et al. 2012; Cai et al. 2016; Cai & Yang 2017). If we can locate the host galaxy by means of EM counterparts, then redshift information on the GW source can be easily obtained. In this paper we simulate GW events based on the Einstein Telescope, the third generation of the ground-based GW detector (The Einstein Telescope Project 2018). Although only a few GW events have been detected by the current advanced ground-based detectors (i.e., the advanced LIGO and Virgo detectors), ET will expand the detection space by three orders of magnitude, and thus will be able to detect many more GW events (Cai et al. 2016; Cai & Yang 2017). In this paper, we carry out a Monte Carlo simulation of the GW signals of NS-NS and NS-BH systems with high signal-to-noise ratio (S/N), based on future observations from the third-generation technology (the “xylophone” configuration; Cai et al. 2016). The specific steps to simulate the mock data are similar to those used in Qi et al. (2019b, 2019). Concerning the error strategy, the combined S/N for the network not only helps us to confirm the detection of GWs with $\rho_{\text{net}} > 8$ —the S/N threshold

Table 1Summary of the Constraints on the “ L - σ ” Relation Parameters Obtained with the Full Sample and Three Subsamples (see Text for Definitions)

Sample (Calibration method + cosmology)	α	κ
Full sample (cosmology-independent method I)	5.10 ± 0.10	33.12 ± 0.15
Full sample (cosmology-independent method II + Planck)	5.13 ± 0.08	33.06 ± 0.13
Full sample (cosmology-independent method II + WMAP9)	5.17 ± 0.09	32.86 ± 0.12
High- z HII Gx (cosmology-independent method I)	5.18 ± 0.65	33.00 ± 1.13
Local HII Gx (cosmology-independent method I)	4.88 ± 0.15	33.48 ± 0.22
GEHRs (cosmology-independent method I)	5.77 ± 0.52	32.25 ± 0.62
High- z HII Gx (cosmology-independent method II)	5.33 ± 0.65	32.70 ± 1.13
Local HII Gx (cosmology-independent method II)	4.93 ± 0.14	33.39 ± 0.22
GEHRs (cosmology-independent method II)	5.81 ± 0.50	32.19 ± 0.61

**Figure 2.** The luminosity distance measurements from 1000 GW events detected by ET.

currently used by the LIGO/Virgo network—but also contributes to the error on the luminosity distance as $\sigma_{D_{L,GW}}^{\text{inst}} \simeq \frac{2D_{L,GW}}{\rho}$ (Zhao et al. 2011). Meanwhile, the lensing uncertainty caused by the weak lensing is also taken into consideration, and is modeled as $\sigma_{D_{L,GW}}^{\text{lens}}/D_{L,GW} = 0.05z$ (Sathyaprakash et al. 2010; Li 2015). Therefore, the distance precision per GW is taken as

$$\begin{aligned} \sigma_{D_{L,GW}} &= \sqrt{(\sigma_{D_{L,GW}}^{\text{inst}})^2 + (\sigma_{D_{L,GW}}^{\text{lens}})^2} \\ &= \sqrt{\left(\frac{2D_{L,GW}}{\rho}\right)^2 + (0.05zD_{L,GW})^2}. \end{aligned} \quad (9)$$

In this paper, we take the flat Λ CDM universe as our fiducial model in the simulation. The matter density parameter $\Omega_m = 0.315$ and the Hubble constant $H_0 = 67.3 \text{ km s}^{-1} \text{ Mpc}^{-1}$ from the latest Planck CMB observations (Planck Collaboration et al. 2018) are taken for Monte Carlo simulations in our analysis. Following the redshift distribution of GW sources taken by Sathyaprakash et al. (2010) and assuming that the luminosity distance measurements obey the Gaussian distribution, the 1000 simulated GW events used for statistical analysis in the next section are shown in Figure 2. In our analysis, in order to get D_L at the redshift of H II galaxy, we have employed the GPs to reconstruct the function $D_{L,GW}(z)$ and its corresponding 1σ uncertainty $\sigma_{D_{L,GW}}$. Distance reconstruction with the simulated GW sample is denoted as “Cosmology-independent method II.”

Now, from the observational point of view, in the framework of the “ L - σ ” relation, the observed distance modulus of an H II object is

$$\mu_{\text{obs}} = 2.5[\kappa + \alpha \log \sigma(\text{H}\beta) - \log F(\text{H}\beta)] - 100.2, \quad (10)$$

with the corresponding error $\sigma_{\mu_{\text{obs}}}$ expressed as $\sigma_{\mu_{\text{obs}}} = \sqrt{(2.5\alpha\sigma_{\log \sigma})^2 + (2.5\sigma_{\log F})^2}$. Here $\sigma_{\log \sigma}$ and $\sigma_{\log F}$ represent the standard errors of the reddening-corrected $\text{H}\beta$ flux ($\log \sigma(\text{H}\beta)$) and the corrected velocity dispersion ($\log F(\text{H}\beta)$). For each H II galaxy, the reconstructed distance modulus μ_{th} can be calculated from the measured redshift z by the definition

$$\mu_{\text{th}} \equiv 5 \log \left[\frac{D_L(z)}{\text{Mpc}} \right] + 25, \quad (11)$$

where $D_L(z)$ is the cosmology-dependent luminosity distance obtained through “Cosmology-independent method I” and “Cosmology-independent method II.” The propagated uncertainty of μ_{th} is given by $\sigma_{\mu_{\text{th}}} = \frac{5\sigma_{D_L}}{D_L \ln 10}$. We determine the parameters (α and κ) characterizing H II objects by minimizing the χ^2 objective function

$$\chi^2(\alpha, \kappa) = \sum_i \frac{(\mu_{\text{obs}}(z_i; \alpha, \kappa) - \mu_{\text{th}}(z_i))^2}{\sigma_{\mu,i}^2} \quad (12)$$

and the corresponding statistical error is given by

$$\sigma^2 = (2.5\alpha\sigma_{\log \sigma})^2 + (2.5\sigma_{\log F})^2 + \left(\frac{5\sigma_{D_L}}{D_L \ln 10} \right)^2. \quad (13)$$

Note that the observational statistical uncertainty for the i th data point and the uncertainty for the reconstructed distance modulus are both included. Then using the Markov Chain Monte Carlo technique available within the CosmoMC package (Lewis & Bridle 2002), we perform Monte Carlo simulations of the posterior likelihood $\mathcal{L} \sim \exp(-\chi^2/2)$ and apply a public Python package “triangle.py” from Foreman-Mackey et al. (2013) to plot our constraint contours.

4. Results and Discussions

In this section, we focus our attention on the constraints on the parameters (α and κ) obtained from different samples, i.e., the full $N = 156$ sample, as well as three subsamples determined from high- z HII Gx, local HII Gx, and GEHRs. The results are summarized in Table 1. The graphic

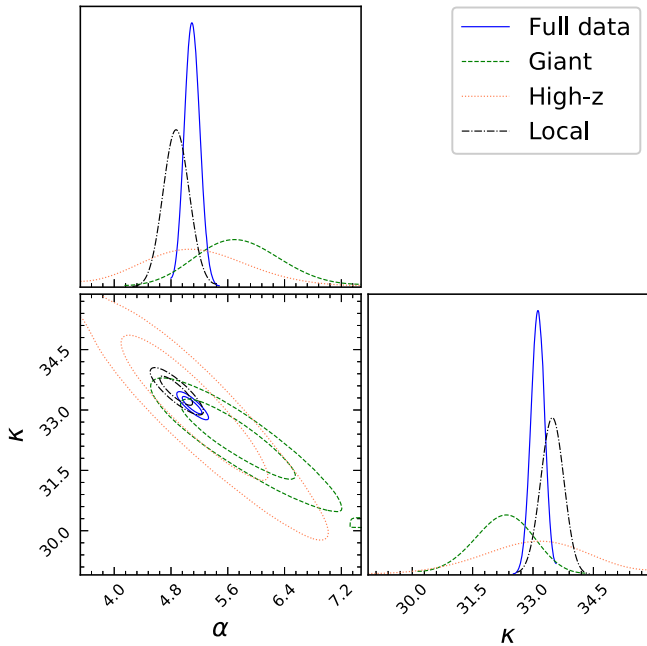


Figure 3. Constraints on H II parameters obtained from the full sample and three subsamples (high- z HII Gx, local HII Gx, and GEHRs), based on the $D_L(z)$ function reconstructed from current $H(z)$ data (“Cosmology-independent method I”).

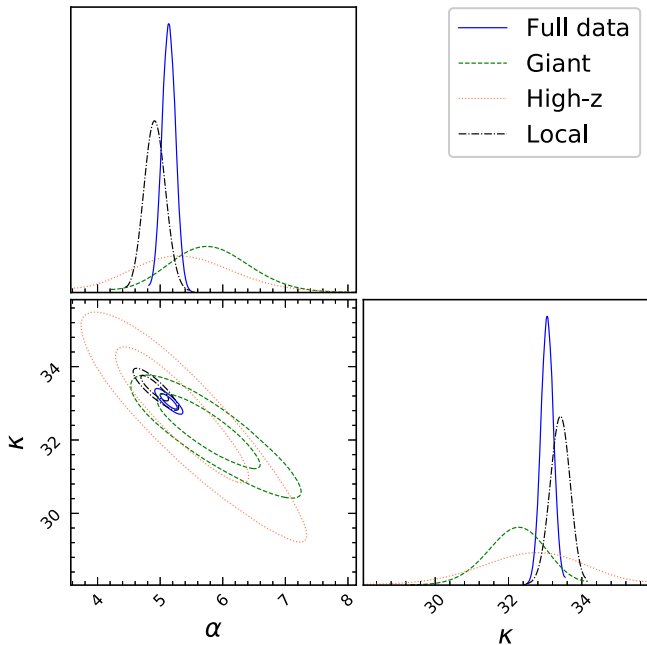


Figure 4. Constraints on H II parameters obtained from the full sample and three subsamples (high- z HII Gx, local HII Gx, and GEHRs), based on the $D_L(z)$ measurements from future simulated GW data (“Cosmology-independent method II”).

representations of the probability distribution of α and κ are presented in Figures 3 and 4, in which one can see the 1D distributions for each parameter and the 1σ and 2σ contours for the joint distribution.

To start with, by applying the above mentioned χ^2 -minimization procedure to the distance reconstruction with the Hubble parameter measurements (“Cosmology-independent method I”), we obtain the results shown in Figure 3.

Performing fits on the full data comprising 156 objects, we obtain the following best-fit values and corresponding 1σ uncertainties (68.3% confidence level):

$$\alpha = 5.10 \pm 0.10, \\ \kappa = 33.12 \pm 0.15.$$

Marginalized 1σ and 2σ contours of each parameter obtained are shown in Figure 3. It is obvious that the full sample analysis has also yielded improved constraints on the meaningful physical parameters, α and κ . More importantly, we find that our constraints on the two parameters with “Cosmology-independent method I” are very different from those obtained in the framework of different cosmologies. For instance, some researchers (Wei et al. 2016) have previously derived a fit to the flat Λ CDM, XCDM, and $Rh = ct$ cosmologies, with the optimized parameter values for the α parameter: $\alpha = 4.89 \pm 0.09$, $\alpha = 4.87 \pm 0.10$, and $\alpha = 4.86 \pm 0.08$, which disagrees with our results at 68.3% confidence level. Therefore, the values of the two best-fit parameters of the phenomenological formula obtained in our analysis, if confirmed by future investigation of H II observations, will offer additional constraints for cosmological tests based on the “ L - σ ” relation of extragalactic sources.

In Table 1 and Figure 3, we show the results of fitting the two parameters, α and κ , on three subsamples described in Section 2. It is interesting to note that the ranges of α and κ for local H II galaxies ($\alpha = 4.88 \pm 0.15$, $\kappa = 33.48 \pm 0.22$) are marginally close to estimates obtained from high- z H II galaxies ($\alpha = 5.18 \pm 0.65$, $\kappa = 33.00 \pm 1.13$). On the other hand, the constrained results for GEHRs, which constitute the most important part of our full H II sample, are particularly interesting. One can clearly see that the best-fit values of the two parameters for this population, $\alpha = 5.77 \pm 0.52$ and $\kappa = 32.25 \pm 0.62$, are significantly different from the corresponding quantities for H II galaxies. That a substantial distinction between α and κ parameters exists for the two subpopulations (GEHRs and HII Gx) is clearer when the 1σ uncertainties are taken into consideration. Consequently, our results indicate the different “ L - σ ” relation of H II regions acting as standard candles.

One issue that might be raised is the choice of the $D_A(z)$ function reconstructed from current $H(z)$ data in the course of our estimation of α and κ . Therefore, we have undertaken a similar analysis with the second model-independent approach, the simulated data of GWs from the third-generation gravitational wave detector.⁵ In this case, performing fits on the full data set, the uncertainties on the two model parameters at the 68.3% confidence level are

$$\alpha = 5.13 \pm 0.08, \\ \kappa = 33.06 \pm 0.13.$$

Figure 4 shows these constraints in the parameter space of α and κ . Comparing constraints based on the two model-independent methods, we see that the confidence regions of α and κ overlap significantly; hence our results and discussions presented above are robust. This tendency could also be found in fits performed on three subsamples with local H II galaxies,

⁵ Note that in the second approach with simulated GW data, we pay more attention to demonstrating the improvements that future GW measurements could provide, concerning the calibration of the “ L - σ ” relation.

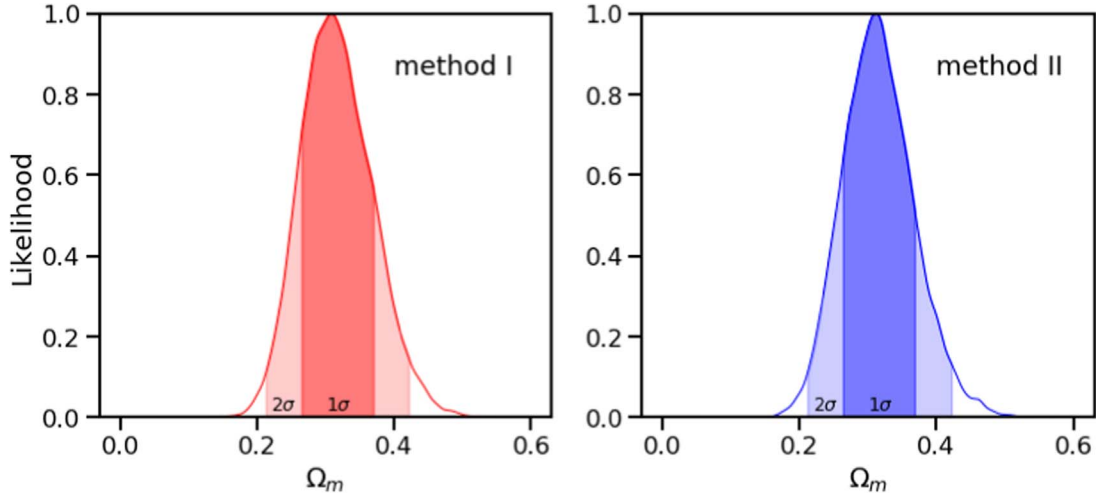


Figure 5. Cosmological fits on the flat Λ CDM model obtained from the full sample, based on the corrected “ L - σ ” relation with the current $H(z)$ data (left panel) and future simulated GW data (right panel).

high- z H II galaxies, and GEHRs. From the results displayed in Figure 4, one can find the obtained values of α and κ from our subsample with GEHRs, whose confidence contours in the (α, κ) parameter plane differ from those of the other two samples. More specifically, in the framework of the “ L - σ ” relation for GEHRs, a lower value of the slope parameter and a higher value of the logarithmic luminosity at $\log \sigma(H\beta) = 0$ are revealed and supported by our analysis. We must keep in mind that a similarity or difference in (α, κ) parameters for H II observations with different types of optical counterparts might reveal similar or different physical processes governing the H β emission in GEHRs and HII Gx. To some extent, our results imply the need to treat these classes of H II observations separately in future cosmological studies.

The second issue that needs clarification is the fiducial cosmology used in our GW simulation, i.e., the consistency between the luminosity distance coming from GP-reconstructed $H(z)$ and the simulated GW standard siren should be fully tested. In order to explore the potential systematics caused by different priors of cosmological parameters, besides assuming a flat Λ CDM model with parameters coming from *Planck* 2018 observations, we also consider the *Wilkinson Microwave Anisotropy Probe* (WMAP) nine-year results (WMAP9) for comparison, in which the matter density parameter and the Hubble constant are respectively taken as $\Omega_m = 0.279$ and $H_0 = 70.0 \text{ km s}^{-1} \text{ Mpc}^{-1}$ (Hinshaw et al. 2013). In this case, the full data set provides the best fit on the “ L - σ ” relation as

$$\begin{aligned}\alpha &= 5.17 \pm 0.09, \\ \kappa &= 32.86 \pm 0.12.\end{aligned}$$

Comparing constraints based on *Planck* and WMAP9 observations shown in Table 1, one could see that the confidence regions of α and κ are almost the same. We remark here that, considering that the WMAP9 and *Planck* data are consistent with sufficient accuracy for comparison with the “ L - σ ” relation, it is not surprising that the regression results of the “ L - σ ” relation in combination with WMAP and *Planck* are compatible in the framework of Λ CDM cosmology (Cao et al. 2015c).

Having performed cosmological-model-independent analysis, we can also investigate cosmological implications of the distance modulus of 156 H II measurements by taking the corrected “ L - σ ” relation into consideration. In this analysis we focus on the Λ CDM model when spatial flatness of the FLRW metric is assumed, which is strongly indicated by the location of the first acoustic peak in the CMB radiation (Planck Collaboration et al. 2018) and also independently supported by the quasar data at $z \sim 3.0$ as demonstrated in Cao et al. (2019). The Friedmann equation is

$$H^2 = H_0^2 [\Omega_m(1+z)^3 + 1 - \Omega_m], \quad (14)$$

where Ω_m parameterizes the density of matter (both baryonic and non-baryonic components) in the universe. For the flat Λ CDM model, unlike the methods used in Wei et al. (2016), we examine the probability distributions of Ω_m by considering the best-fitted α and β parameters (with their 1σ uncertainties) obtained from the previous model-independent tests. Fitting the Λ CDM model to the full sample with the corrected “ L - σ ” relation, one is able to get observational constraints on the matter density parameter as $\Omega_m = 0.314 \pm 0.054$ (calibrated with standard clocks in the EM domain) and $\Omega_m = 0.311 \pm 0.049$ (calibrated with standard sirens in the GW domain). The results are shown in Figure 5. On the one hand, one may observe that the results obtained from the combined H II sample are consistent with the fit based on the full-mission *Planck* observations of temperature and polarization anisotropies of the CMB radiation (Planck Collaboration et al. 2018), as well as with a newly compiled data set of milliarcsecond compact radio sources representing intermediate-luminosity quasars covering the redshift range $0.5 < z < 2.8$ (Cao et al. 2017a, 2017b; Li et al. 2017; Xu et al. 2018). On the other hand, our results strongly suggest that the dynamical properties of H II galaxies may significantly impact the likelihood distributions of Ω_m and thus constraints on the properties of dark energy. This conclusion is strengthened by the comparison of our cosmological fits from the recalibrated “ L - σ ” relation through our cosmological-model-independent tests and those based on a specific cosmological scenario (Wei et al. 2016). Therefore, although

the constraints resulting from this analysis are marginally consistent with the previous works, our results based on a cosmological-model-independent check (especially “Cosmology-independent method I”) could be useful as hints for priors on α and κ parameters in future cosmological studies using H II observations.

5. Conclusion

In this paper, we explored the properties of a sample of 156 H II galaxies (HII Gx) and giant extragalactic H II regions (GEHRs) with measured flux density and turbulent gas velocity. The “ L - σ ” relation of these standard candles is usually parameterized as $\log L(\text{H}\beta) = \alpha \log \sigma(\text{H}\beta) + \kappa$. Using the cosmological distances reconstructed through two new cosmology-independent methods, we investigate the correlation between the emission-line luminosity L and ionized gas velocity dispersion σ . The method is based on non-parametric reconstruction using the measurements of Hubble parameters from cosmic clocks, as well as the simulated data of GWs from the third-generation gravitational wave detector (the Einstein Telescope), which can be considered as standard sirens. Moreover, we have also investigated cosmological implications of the distance modulus of 156 H II measurements by taking the corrected “ L - σ ” relation into consideration, which encourages us to probe cosmological parameters beyond the current reach of Type Ia supernovae. Here we summarize our main conclusions in more detail.

1. In the full sample, we find that measurements of HII Gx and GEHRs provide tighter estimates of the “ L - σ ” relation parameters. Performing fits on the full data comprising 156 objects, we obtain the following best-fit values and corresponding 1σ uncertainties (68.3% confidence level): $\alpha = 5.10 \pm 0.10$, $\kappa = 33.12 \pm 0.15$ (calibrated with standard clocks in the EM domain) and $\alpha = 5.13 \pm 0.08$, $\kappa = 33.06 \pm 0.13$ (calibrated with standard sirens in the GW domain). We have also explored the potential systematics caused by different priors of cosmological parameters in a GW simulation. In the framework of a flat Λ CDM model with parameters coming from WMAP9, the full data set provides the best fit to the “ L - σ ” relation: $\alpha = 5.17 \pm 0.09$ and $\kappa = 32.86 \pm 0.12$ (calibrated with standard sirens in the GW domain). More importantly, our constraints on the two parameters with two new cosmology-independent methods are very different from those obtained in the framework of different cosmologies.
2. Furthermore, we divide the full sample into three different subsamples according to their optical counterparts. It turns out that the ranges of α and κ for local H II galaxies are marginally close to estimates obtained from high- z H II galaxies. The best-fit values for GEHRs are significantly different from the corresponding quantities for H II galaxies. That substantial distinction between α and κ parameters exists for the two subpopulations (GEHRs and HII Gx) is clearer when the 1σ uncertainties are taken into consideration. Consequently, closeness or difference of parameter values for different types of counterparts indicates a similar or different “ L - σ ” relation of H II regions acting as standard candles, as well as the existence of possible similar or different physical

processes governing the $\text{H}\beta$ emission in GEHRs and HII Gx.

3. Fitting the Λ CDM model to the full sample with the corrected “ L - σ ” relation, one is able to get observational constraints on the matter density parameter as $\Omega_m = 0.314 \pm 0.054$ and $\Omega_m = 0.311 \pm 0.049$, which are inconsistent with the previous results obtained on the same sample but agree very well with other recent astrophysical measurements including *Planck* observations. Therefore, it is strongly suggested that reliable knowledge of the dynamical properties of H II galaxies may significantly impact the constraints on relevant cosmological parameters. The values of the two best-fit parameters of the “ L - σ ” relation obtained in our analysis, if confirmed by future investigation of H II observations, will offer additional constraints for cosmological tests based on extragalactic sources.
4. As a final remark, we point out that the sample discussed in this paper is based on H II objects discovered in different surveys. Our analysis potentially may suffer from systematics stemming from this inhomogeneity. Therefore, we may expect stronger and more convincing constraints on the dynamical properties of H II galaxies in the coming years with more precise data, especially a larger sample of high- z HII Gx observed by current facilities such as the K -band Multi-Object Spectrograph at the Very Large Telescope (Terlevich et al. 2015).

We are grateful to Jingzhao Qi for helpful discussions. This work was supported by National Key R&D Program of China No. 2017YFA0402600, the National Natural Science Foundation of China under grants Nos. 11503001, 11690023, 11373014, and 11633001, the Strategic Priority Research Program of the Chinese Academy of Sciences, grant No. XDB23000000, the Interdisciplinary Research Funds of Beijing Normal University, and the Opening Project of Key Laboratory of Computational Astrophysics, National Astronomical Observatories, Chinese Academy of Sciences.

ORCID iDs

Shuo Cao  <https://orcid.org/0000-0002-8870-981X>

References

- Abazajian, K. N., Adelman-McCarthy, J. K., Agüeros, M. A., et al. 2009, *ApJS*, **182**, 543
- Abbott, B., Abbott, R., Abbott, T. D., et al. 2017, *Natur*, **551**, 85
- Abbott, B. P., Abbott, R., Abbott, T. D., et al. 2016, *PhRvL*, **116**, 061102
- Bergeron, J. 1977, *ApJ*, **211**, 62
- Biesiada, M., Piórkowska, A., & Malec, B. 2010, *MNRAS*, **406**, 1055
- Bordalo, V., & Telles, E. 2011, *ApJ*, **735**, 52
- Bosch, G., Terlevich, E., & Terlevich, R. 2002, *MNRAS*, **329**, 481
- Cai, R.-G., Guo, Z.-K., & Yang, T. 2016, *PhRvD*, **93**, 043517
- Cai, R.-G., & Yang, T. 2017, *PhRvD*, **95**, 044024
- Calzetti, D., Armus, L., Bohlin, R. C., et al. 2000, *ApJ*, **533**, 682
- Cao, S., Biesiada, M., Gavazzi, R., Piórkowska, A., & Zhu, Z.-H. 2015b, *ApJ*, **806**, 185
- Cao, S., Biesiada, M., Jackson, J., et al. 2017a, *JCAP*, **02**, 012
- Cao, S., Biesiada, M., Qi, J., et al. 2018, *EPJC*, **78**, 749
- Cao, S., Biesiada, M., Yao, M., & Zhu, Z.-H. 2016, *MNRAS*, **461**, 2192
- Cao, S., Biesiada, M., Zheng, X., & Zhu, Z.-H. 2015c, *ApJ*, **806**, 66
- Cao, S., Chen, Y., Zhang, J., & Ma, Y. 2015a, *IJTP*, **54**, 1492
- Cao, S., & Liang, N. 2013, *IJMPD*, **22**, 1350082
- Cao, S., Liang, N., & Zhu, Z.-H. 2011, *MNRAS*, **416**, 1099
- Cao, S., Qi, J., Biesiada, M., et al. 2019, *PDU*, **24**, 100274
- Cao, S., Zheng, X., Biesiada, M., et al. 2017b, *A&A*, **606**, A15

- Chávez, R., Terlevich, E., Terlevich, R., et al. 2012, *MNRAS*, **425**, L56
- Chávez, R., Terlevich, R., Terlevich, E., et al. 2014, *MNRAS*, **442**, 3565
- Chen, Y., Geng, C.-Q., Cao, S., Huang, Y.-M., & Zhu, Z.-H. 2015, *JCAP*, **02**, 010
- Dalal, N., Holz, D. E., Hughes, S. A., & Jain, B. 2006, *PhRvD*, **74**, 063006
- Dottori, H. A. 1981, *Ap&SS*, **80**, 267
- Dottori, H. A., & Bica, E. L. D. 1981, *A&A*, **102**, 245
- Erb, D. K., Steidel, C. C., Shapley, A. E., et al. 2006a, *ApJ*, **647**, 128
- Erb, D. K., Steidel, C. C., Shapley, A. E., et al. 2006b, *ApJ*, **646**, 107
- Foreman-Mackey, D., Hogg, D. W., Lang, D., & Goodman, J. 2013, *PASP*, **125**, 306
- Fuentes-Masip, O., Muñoz-Tuñón, C., Castañeda, H. O., & Tenorio-Tagle, G. 2000, *AJ*, **120**, 752
- García-Díaz, M. T., Henney, W. J., López, J. A., & Doi, T. 2008, *RMxAA*, **44**, 181
- Hinshaw, G., Larson, D., Komatsu, E., et al. 2013, *ApJS*, **208**, 19
- Holanda, R. F. L., Carvalho, J. C., & Alcaniz, J. S. 2013, *JCAP*, **2013**, 027
- Holsclaw, T., Alam, U., Sansó, B., et al. 2010, *PhRvL*, **105**, 241302
- Jarosik, N., Bennett, C. L., Dunkley, J., et al. 2011, *ApJS*, **192**, 14
- Kunth, D., & Östlin, G. 2000, *A&ARv*, **10**, 1
- Lewis, A., & Bridle, S. 2002, *PhRvD*, **66**, 103511
- Li, T. G. 2015, *Extracting Physics from Gravitational Waves* (Berlin: Springer)
- Li, X. L., Cao, S., Zheng, X., et al. 2017, *EPJC*, **77**, 677
- Liao, K., Avgoustidis, A., & Li, Z. 2015, *PhRvD*, **92**, 123539
- Ma, Y., Cao, S., Zhang, J., et al. 2019, *EPJC*, **79**, 121
- Mania, D., & Ratra, B. 2012, *PhLB*, **715**, 9
- Masters, D., McCarthy, P., Siana, B., et al. 2014, *ApJ*, **785**, 153
- Melia, F. 2007, *MNRAS*, **382**, 1917
- Melia, F. 2013, *A&A*, **553**, A76
- Melnick, J. 1979, *ApJ*, **228**, 112
- Melnick, J., Moles, M., Terlevich, R., & Garcia-Pelayo, J.-M. 1987, *MNRAS*, **226**, 849
- Melnick, J., Terlevich, R., & Moles, M. 1988, *MNRAS*, **235**, 297
- Melnick, J., Terlevich, R., & Terlevich, E. 2000, *MNRAS*, **311**, 629
- Pan, Y., Gong, Y., Cao, S., Gao, H., & Zhu, Z.-H. 2015, *ApJ*, **808**, 78
- Perlmutter, S., Aldering, G., Goldhaber, G., et al. 1999, *ApJ*, **517**, 565
- Pettini, M., Kellogg, M., Steidel, C. C., et al. 1998, *ApJ*, **508**, 539
- Planck Collaboration, Aghanim, N., Akrami, Y., et al. 2018, arXiv:1807.06209
- Plionis, M., Terlevich, R., Basilakos, S., et al. 2011, *MNRAS*, **416**, 2981
- Qi, J.-Z., Cao, S., Biesiada, M., et al. 2018, *RAA*, **18**, 66
- Qi, J. Z., Cao, S., Pan, Y., & Li, J. 2019, *PDU*, **26**, 100338
- Qi, J.-Z., Cao, S., Zhang, S., et al. 2019a, *MNRAS*, **483**, 1104
- Qi, J. Z., Cao, S., Zheng, C., et al. 2019b, *PhRvD*, **99**, 063507
- Riess, A. G., Filippenko, A. V., Challis, P., et al. 1998, *ApJ*, **116**, 1009
- Sathyaprakash, B., Schutz, B. F., & Van Den Broeck, C. 2010, *CQG*, **27**, 215006
- Schutz, B. F. 1986, *Natur*, **323**, 310
- Searle, L., & Sargent, W. L. W. 1972, *ApJ*, **173**, 25
- Seikel, M., Clarkson, C., & Smith, M. 2012a, *JCAP*, **6**, 036
- Seikel, M., Yahya, S., Maartens, R., & Clarkson, C. 2012b, *PhRvD*, **86**, 083001
- Siegel, E. R., Guzmán, R., Gallego, J. P., Orduña López, M., & Rodríguez Hidalgo, P. 2005, *MNRAS*, **356**, 1117
- Taylor, S. R., Gair, J. R., & Mandel, I. 2012, *PhRvD*, **85**, 023535
- Telles, E. 2003, in ASP Conf. Proc. 297, *Star Formation Through Time*, ed. E. Perez, R. M. Gonzalez Delgado, & G. Tenorio-Tagle (San Francisco, CA: ASP), 143
- Terlevich, R., & Melnick, J. 1981, *MNRAS*, **195**, 839
- Terlevich, R., Terlevich, E., Melnick, J., et al. 2015, *MNRAS*, **451**, 3001
- The Einstein Telescope Project 2018, Einstein Telescope, <https://www.et-gw.eu/et/>
- Wei, J.-J., Wu, X.-F., & Melia, F. 2016, *MNRAS*, **463**, 1144
- Xu, T.-P., Cao, S., Qi, J., et al. 2018, *JCAP*, **06**, 042
- Yang, T., Guo, Z.-K., & Cai, R.-G. 2015, *PhRvD*, **91**, 123533
- Zhao, W., Van Den Broeck, C., Baskaran, D., & Li, T. 2011, *PhRvD*, **83**, 023005
- Zheng, X.-G., Qi, J.-Z., Cao, S., et al. 2019, *EPJC*, **79**, 637